Journal of Infrastructure Preservation and Resilience

RESEARCH Open Access

Water absorptivity and frost resistance performance of self-ignition coal gangue autoclaved aerated concrete

Xinyu Cong[1], Yiqiu Tan[1], Shuang Lu[2,3*], Zhaojia Wang[4*] and Tianyong Huang[4]

Abstract

Self-ignition coal gangue (SCG) used as one of precursors to fabricate autoclaved aerated concrete (AAC). Aiming at studying water absorptivity and frost resistance performance of SCG-based AAC (SCGAAC), three-period water absorption tests and freeze-thaw tests were carried out and the corresponding results were recorded and analyzed. In order to modify the water absorptivity of SCGAAC, foam stabilizer was applied to adjust pore structure while calcium stearate was expected to change hydrophilic feature of SCG. It was demonstrated that the compressive strength of SCGAAC containing foam stabilizer or calcium stearate declined at different levels. For water absorption, foam stabilizer failed to decrease the water content and even increased water absorption rates. Calcium stearate controlled water absorption rate successfully although the ultimate water content hardly reduced. All of the SCGA AC samples exhibited intact appearance after 50 freeze-thaw cycles and showed excellent frost resistance performance. Three models were proposed to predict water absorptivity and frost resistance performance of SCGA AC and the corresponding prediction results matched test resulted well.

Keywords: Self-ignition coal gangue, Autoclaved aerated concrete, Porosity, Water absorptivity, Frost resistance performance

Introduction

Autoclaved aerated concrete (AAC) has been commonly used as construction material by virtue of its functional performance [1–6], in particular, thermal insulation and energy efficiency [7–9]. AAC comprised of cement, fly ash, lime and fine-grained aggregates has been produced in Asia, Europe and Americas since it once turned into creation in Sweden in 1930s [10]. In recent years, porous and light concrete has been used to replace the traditional soil in subgrade construction due to the porous concrete subgrade showed the better stiffness and lighter mass to avoid settlement deformation when roads were in service. AAC with abundant pores is expected to be an alternative in subgrade construction. However, the excellent stiffness of AAC would be shadowed when the porous material suffers high water absorption and frost damage. The mass loss and compressive strength loss of water-saturated AAC reached 1.5% and 16.6% after 50 freeze-thaw cycles. Frost resistance of AAC deteriorated with the interior moisture increasing and it was easy to generate frost-heaving cracks and denudation. However, Miloš Jerman [11] observed that freeze/thaw resistance of capillary saturated AAC samples was satisfactory up to 25 cycles, and, the AAC with moisture content lower than 10% can successfully resist to 50 cycles. Water content and sorptivity showed a strong impact on AAC performance, especially on strength and frost resistance, which are influential in subgrade structure.

As a porous product, pore structure has a strong effect on the moisture distribution of AAC. In the past few decades, some principles related to water migration in

* Correspondence: hitlu@126.com; wangzhaojia@bbmg.com.cn
[2]School of Civil Engineering, Harbin Institute of technology, Harbin 150090, China
[4]State Key Laboratory of Solid Waste Reuse for Building Materials, Beijing Building 11 Materials Academy of Science Research, Beijing 100041, China
Full list of author information is available at the end of the article

porous AAC system were presented [11–14]. For example, it was found that water vapor diffusion and capillary suction dominated in dry conditions and high humidity circumstances, respectively. Water absorption and migration caused by capillarity in porous materials like AAC were defined as a sorptivity process which was governed by the unsaturated flow theory [8]. The overall capillary absorption was well described as two processes: a capillary absorption in aerated pores achieved gravitational equilibrium rapidly; and a slow capillary absorption into the matrix pores [15].

Coal gangue (CG) is a type of waste produced during the coal mining process, which wifely stacks around ore fields. The CG stacks are prone to self-ignite because of combustible component in CG, and self-ignition coal gangue (SCG) is generated. With the intention of consuming self-ignition coal gangue (SCG) effectively, SCG was innovatively used as a precursor of AAC to fabricated SCG-based AAC (SCGAAC) [16]. Actually, SCG is a type of aluminum-rich cementitious materials with high active ingredients. Aluminum-rich tobermorite by replacing Si^{4+} with Al^{3+} was generated in SCGAAC improving microstructure and macro properties. SCGAAC with good compressive strength and stiffness is expected to solve the uniform deformation problem in subgrade structure, while SCGAAC consuming abundant tailings and saving tons of cement is instrumental in reducing foot print of infrastructure engineering.

For the application of SCGAAC subgrade, it is of importance to modify the water absorption and frost resistance of SCGAAC. In this study, two different chemical agents were used to improve SCGAAC performance on water absorption and frost resistance. Specifically, the compressive strength and mass change of SCGAAC subjected to freeze-thaw cycles were tested and the corresponding prediction models relevant to porosity were proposed.

Materials and experiments

Raw materials

The precursors of SCGAAC comprised of SCG, ordinary Portland cement (PC), lime (L) and gypsum (G). The chemical composition of the raw materials was listed in Table 1. In this study, the SCG was resourced from Heilongjiang, China. The as-received SCG aggregates with a particle size of 10–30 mm were milled to form SCG powder which sieved through an 80 μm sieve. Naphthalene-based superplasticizer (FDN) was selected to adjust the slump flow (SF) of SCGAAC pastes. Aluminum powder (AP) was used as a foaming agent in AAC system.

Chemical agents and mix ratios

Two chemical admixtures added into the mixes when fabricating SCGAAC samples. A foam stabilizer (F) was used to reduce bubble cracking during the stirring process and optimize pore structure of hardened AAC. The foam stabilizer was a type of surfactant which dispersed aluminium paste in the slurry and produced bubbles of similar size. Meanwhile, the foam stabilizer shrank the bubble size to balance the pressure inside and outside easily and to reduce cracking bubbles during the stirring and setting stages. The other chemical agent, calcium stearate (C), was regarded as a waterproof agent to decrease water absorption. The two chemical agents were expected to reduce water absorption in different ways. In order to improve the pore structure of AAC, the foam stabilizer was applied to avoid bubbles merging and to reduce interconnected pores. In addition, calcium stearate achieved a hydrophobic AAC matrix that was instrumental in absorbing little water. The dosage of the chemical agents and the mix ratios of SCGAAC were presented in Table 2.

Specimens

The mix procedures of SCGAAC was applied as the method mentioned in a preceding study [16]. Slump flow (SF) was a measurement index reflecting workability of fresh AAC pastes and it was found that the SF had an influence on the density and pore structure of hardened AAC [16]. In this study, all of the fresh pastes were controlled the SF at 250, 290 and 320 (±5) mm respectively through adjusting the dosage of FDN. The SCGA AC samples were moulded in 100 mm^3cube metal moulds. The fabrication process and the curing protocol referred to [16].

Test methods

Super depth of field microscope (SDFM) was applied to characterize the pore structure of SCGAAC. In order to accurately identify the pores and matrix, the samples for the pore characterization were pretreated. In order to

Table 1 Chemical composition and loss on ignition of precursors

Oxide (wt.%)	CaO	SiO_2	Al_2O_3	Fe_2O_3	MgO	SO_3	Loss on ignition
SCG	1.18	61.02	23.55	6.70	0.52	–	2.5
PC	62.31	21.05	5.50	3.92	1.72	2.66	–
L	85.33	3.28	–	–	5.20	–	–
G	29.93	7.31	11.70	0.60	0.18	38.84	9.62

Table 2 Mix proportions of SCGAAC

SCG (g)	L (g)	PC (g)	G (g)	AP		W/P[a]
				(‰)	(g)	
1300	559	481	78	1.3	3.14	0.50
Label	Chemical agents		SE (mm)	FDN		ρ^b (kg/m3)
	type	(g)		(%)	(g)	
f-1	–	–	250	1.40	33.85	750
f-2	–	–	290	1.60	38.69	635
f-3	–	–	320	1.80	43.52	634
f-4	F	0.15	250	1.40	33.85	704
f-5	F	0.15	290	1.60	38.69	710
f-6	F	0.15	320	1.80	43.52	693
f-7	C	72.5	250	1.60	38.69	660
f-8	C	72.5	290	1.70	41.11	658
f-9	C	72.5	320	1.85	44.73	613

[a]W/P represents water-to-precursor ratio;
[b]ρ represents SCGAAC density

form a contrast between the matrix and the pores, as shown in Fig. 1, the SCGAAC sample was painted in black and the pores were filled with titanium dioxide powder. The images of the SCGAAC samples were captured by the camera of the SDFM and processed in the dark field environment.

Compressive strength results were obtained from testing SCGAAC cubes with 10 (±2) wt% water content. For the water absorption tests, drying treatment at 105 ± 5 °C for 24 h was performed before absorptivity tests. Figure 2 exhibited the testing procedure for the water absorption behavior of the SCGAAC samples. The water was periodically added into a tank to soak the pre-dried samples. Specifically, the depth of water for the first 24-h absorption test was as high as 3 cm and the mass change of the samples were recorded. The water depths for the second and third 24-h absorption tests were assigned at 7 cm and 12 cm, respectively.

The measuring process of water content and saturated water absorptivity conforms to *GB/T 11969–2008* [17]. The water absorptivity W_R can be calculated as Eq. (1):

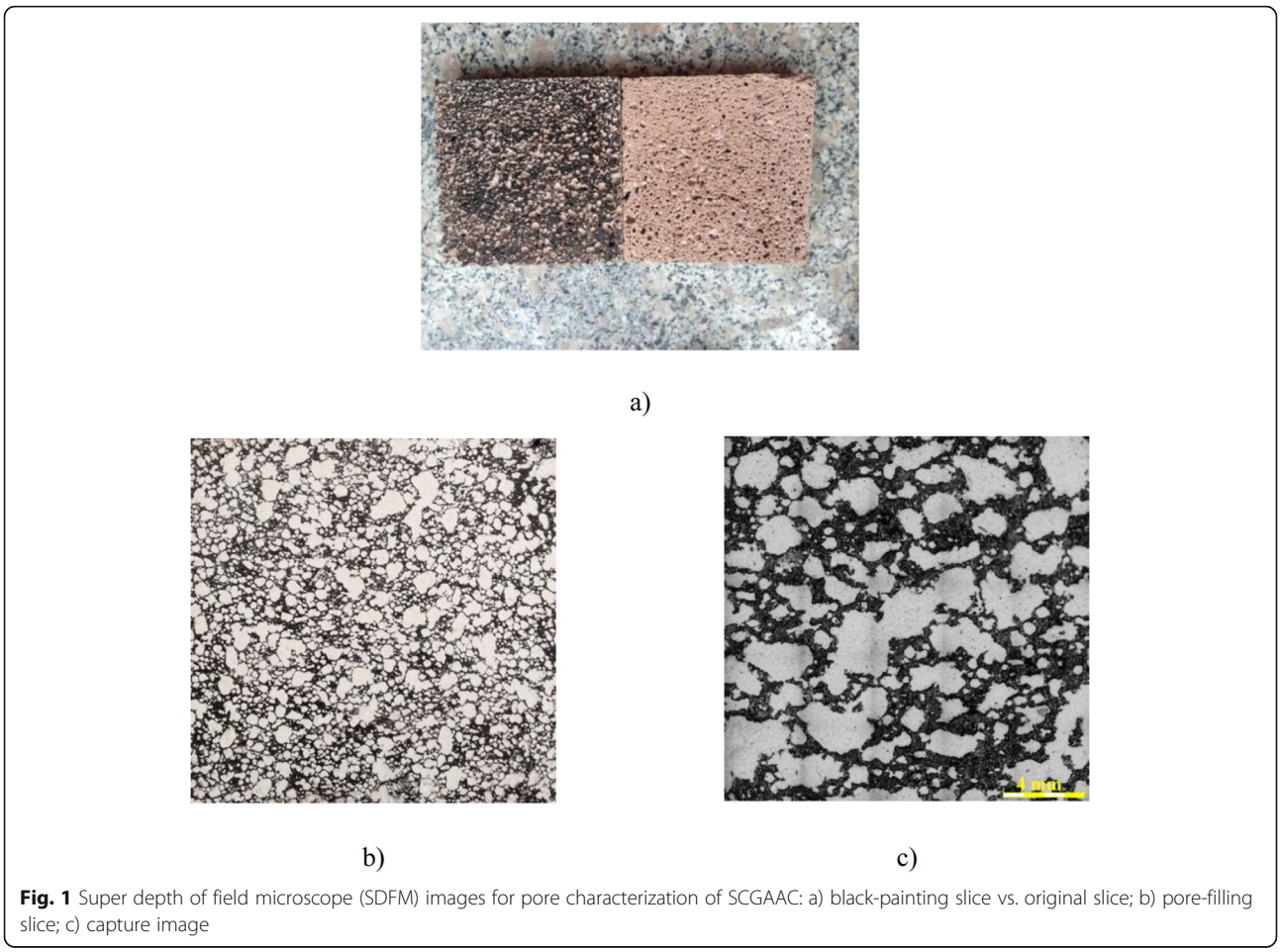

Fig. 1 Super depth of field microscope (SDFM) images for pore characterization of SCGAAC: a) black-painting slice vs. original slice; b) pore-filling slice; c) capture image

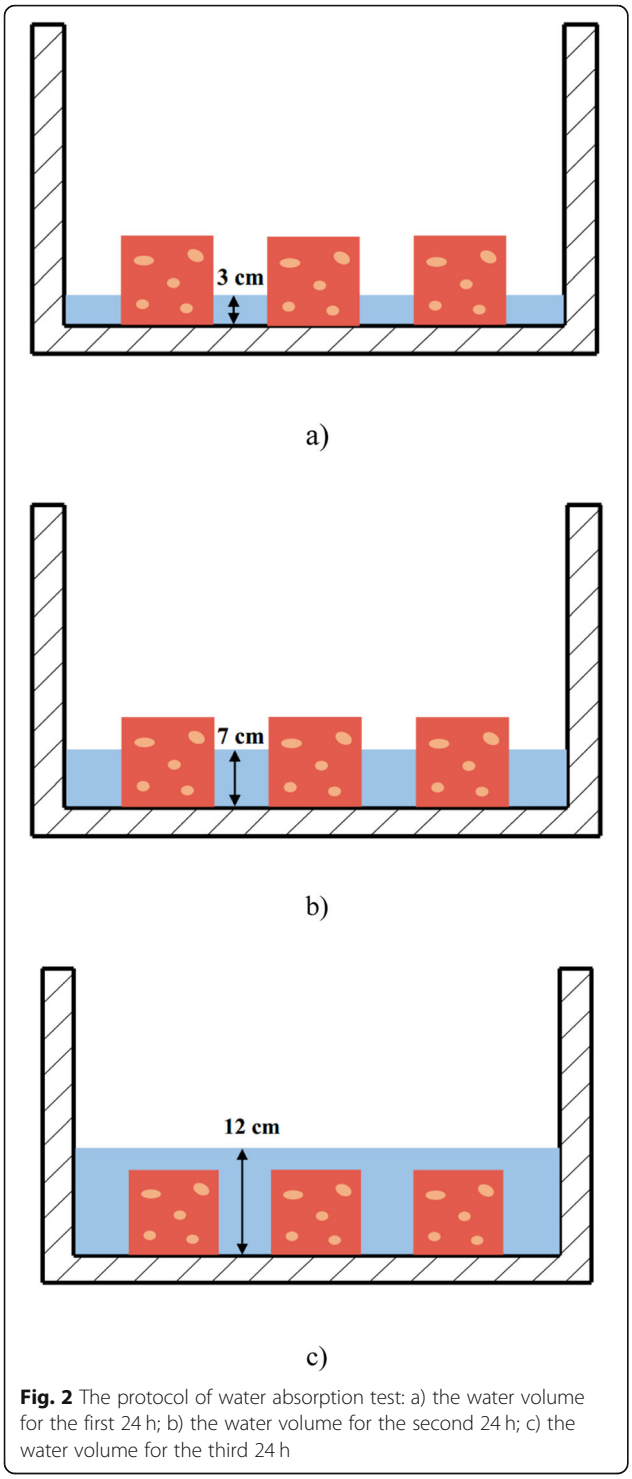

Fig. 2 The protocol of water absorption test: a) the water volume for the first 24 h; b) the water volume for the second 24 h; c) the water volume for the third 24 h

$$W_R = \frac{M_g - M_0}{M_0} \times 100\% \quad (1)$$

where M_g is the mass of sample after water absorption and M_0 is the mass of sample in absolute dry status.

Frost resistance performance of SCGACC was tested according to *GB/T 11969–2008* [17]. One freezing and thawing cycle contained two stages: the water-soaked samples froze in air at − 20 ± 2 °C for 4 h; and then the temperature rose to 20 ± 2 °C and the samples immerged in water for 4 h to thaw. The compressive strength and mass change were recorded after the SCGAAC samples were subjected to 50 freezing and thawing cycles.

Results and discussion

Pore structure of SCGAAC

According to the captured pictures of SCGAAC slices, three main pore parameters were computed by the OLYMPUS Stream software connected with the SDFM, including porosity, pore-size distribution and average length-width ratio (ALwR) of the pores. The results related to the pores of the SCGAAC samples were shown in Table 3. It was observed that porosity increased with the sample SF becoming larger. For the samples without any chemical agents, the porosity rose by approximate 16% when the SF increased from 250 mm to 320 mm. The f-1 sample showed the lowest pore content (45.93%) and the highest density (750 kg/m^3). The porosity increased obviously as the SF was enlarged, especially the percentage of the pores within 0.5–2 mm.

The chemical agents improved the pore structure of SCGAAC at different levels through lowering the porosity and mesopores. The foam stabilizer was a type of surfactant that reduced the surface tension of the slurry and forming stable bubbles. Much more bubbles formed and existed easily in the thick slurry with 250 mm SF when the F agent was used. As the slurry becoming thinner (320 mm SE), a part of bubbles inclined to merge and crack in low viscosity pastes. The F agent made the slurry hold the bubble in a steady status to avoid bubble mergence. Hence, the F agent adjusted the bubble status and content in the slurry with different SF and the thick slurry witnessed an obvious effectiveness. The agent C also showed an effect on adjusting pore structure of the SCGAAC samples. For all of the samples with different

Table 3 Characterization of pores in SCGAAC

Label	Porosity (%)	Pore-size distribution (%)			ALwR
		Fine pore <0.5 mm	Mesopore 0.5 ~ 2 mm	Large pore >2 mm	
f-1	45.93	2.68	94.89	2.43	1.61
f-2	56.17	2.43	92.16	5.41	1.70
f-3	62.82	6.58	89.69	3.73	1.65
f-4	54.33	3.25	89.79	6.96	1.65
f-5	57.55	3.85	89.51	6.64	1.60
f-6	58.96	3.64	89.26	6.92	1.65
f-7	53.06	4.34	87.26	8.40	1.65
f-8	54.87	5.07	86.87	8.06	1.61
f-9	55.39	4.98	87.26	7.76	1.61

SE, the samples containing the C agent had a lower porosity than those containing the F agent. It was found that the small and large pores increased while the mesopores reduced.

ALwR was a parameter reflected the degree of pores connecting. Assuming that independent bubbles in the slurry were sphere and the ALwR equals 1 if there is no any connection happening among the bubbles. The ALwR exceeds 1 when the bubbles merge near a direction. Therefore, this parameter is an index for understanding the connection degree of pores in the SCGA AC. The ALwR results showed no obvious relationships with the porosity results. It was worth noting that the SCGAAC including the C agent had the lowest ALwR values at any SF levels, especially for the thin slurry samples.

Mechanical properties of SCGAAC

Compressive strength was tested to assess the mechanical properties of the SCGAAC. As exhibited in Fig. 3, the chemical admixtures showed an influence on the compressive strength. The foam stabilizer almost brought no harm in compressive strength of the SCGA AC while calcium stearate obviously decreased the compressive strength. This was because that the density of the SCGAAC containing calcium stearate was lower than that of the others. The corresponding density results were listed in Table 2. The foam stabilizer kept small bubbles suspending in the slurry rather than rising up and cracking through adjusting the surface tension of fresh slurry. The bubbles evenly distributed in the matrix to form relatively dense system, which resulted in the high compressive strength.

Compared to the admixture free samples, the compressive strength of the SCGAAC comprising the agent C declined visibly. The compressive strength was even lower than 4.0 MPa when the SF was over 290 mm. The

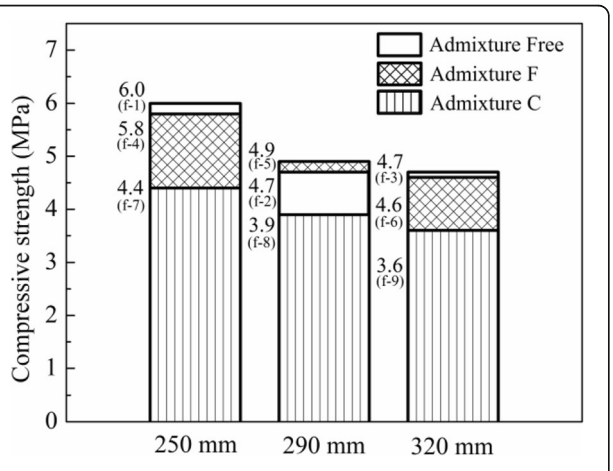

Fig. 3 Compressive strength of SCGAAC

SCGAAC containing the agent C with the lowest porosity, according to the pore parameters presented in Table 3, had the lowest density. It was reasonable to infer that calcium stearate had a negative influence on the matrix of SCGAAC.

Water absorptivity of SCGAAC

Water-absorbing rates of the SCGAAC samples were shown in Fig. 4. The water absorption curves for the f-1, f-2 and f-3 presented the identical trends. During the three water uptake periods, the samples with the 290 mm SF obtained the highest water content. The water content of these three samples after 72-h absorbing were at a similar level, ranging from 47.3% to 52.3%. Although the foam stabilizer enhanced the compressive strength, the water absorptivity failed to be controlled by using the foam stabilizer. As shown in Fig. 4, f-4, f-5 and f-6 absorbed more volume of water in every period compared to the counterparts without any admixture. For the f-6 sample, the water content after 72 h was slightly lower than 60%. Two potential reasons explain this results. The first one is the formation of interconnecting capillary pores because of using the foam stabilizer, and the other one is the matrix becoming more hydrophilic.

Compared to the foam stabilizer, calcium stearate effectively controlled the water absorption of the SCGA AC within 48 h. Although the 72-h water contents were near the others, the water-uptake of the SCGAAC comprising calcium stearate was obviously slow during the first 24 h. Calcium stearate was a strong waterproof agent for the SCGAAC, which can be seen according to the slopes of water absorption curves in Fig. 4. For the samples f-1 to f-6, the water absorption rates were variable over the three periods, where the initial water uptake slopes were steep and the rates gradually tended to be flat at last. When it came to the samples with calcium stearate, the trend of water absorption was different. The samples kept absorbing water with an invariable rate over the whole duration. The lowest water absorption of the SCGAAC came from the f-8 sample with 37.9% of the water content after 72 h.

The different trend of water absorption was mainly from hydrophobicity caused by calcium stearate. It was difficult for water to infiltrate into the CG matrix when the water was initially on contact with the matrix. It took time to permeate into the matrix during the immerging period. For the samples modified by calcium stearate, moisture transport along the pore path because of capillarity was a minor factor for water absorption process. Although the driving force for water uptake was capillarity, it was water-holding capacity that decided how much moisture can be transported up. The SCGA AC samples without calcium stearate absorbed water quickly when water was on contact with the matrix and

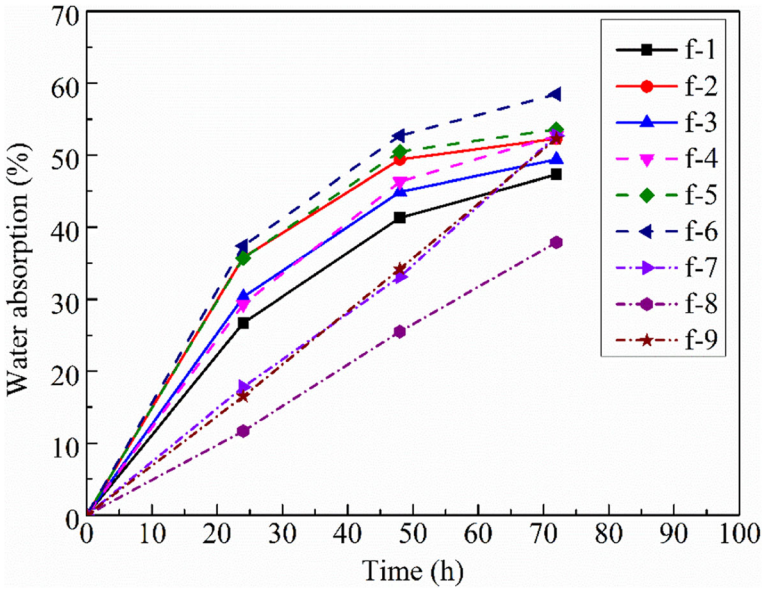

Fig. 4 Water absorptivity of SCGAAC

the water content for the local matrix under the water line nearly reached saturation over the first period. The rate of moisture transport was slower than that of water uptake, therefore, the curves for f-1 to f-6 showed decreased slopes. For the f-7 to f-9 samples, water absorption rates kept a constant throughout, which demonstrated that the water content for the matrix was unsaturated and it reached a dynamic equilibrium between the moisture transport and water uptake. Therefore, calcium stearate was an effective waterproof agent for SCGAAC and it was efficient to decrease water absorption rate and reduce water content at early time.

Frost resistance of SCGAAC

Figures 5 and 6 showed the mass change ($\Delta m/m$) and compressive strength change of the SCGAAC samples subjected to freeze-thaw cycles. The $\Delta m/m$ results of the samples after 25 cycles were exhibited in Fig. 5 (a). All of the samples showed an increased mass after 25 freeze-thaw cycles and the highest increment reached 6.53% from the f-8 samples. It was worth noting that the SCGAAC with calcium stearate increased more mass than the other two types of SCGAAC in any SF status. Combined with the water absorption curves shown in Fig. 4, it can be inferred that the f-7 to f-9 samples being

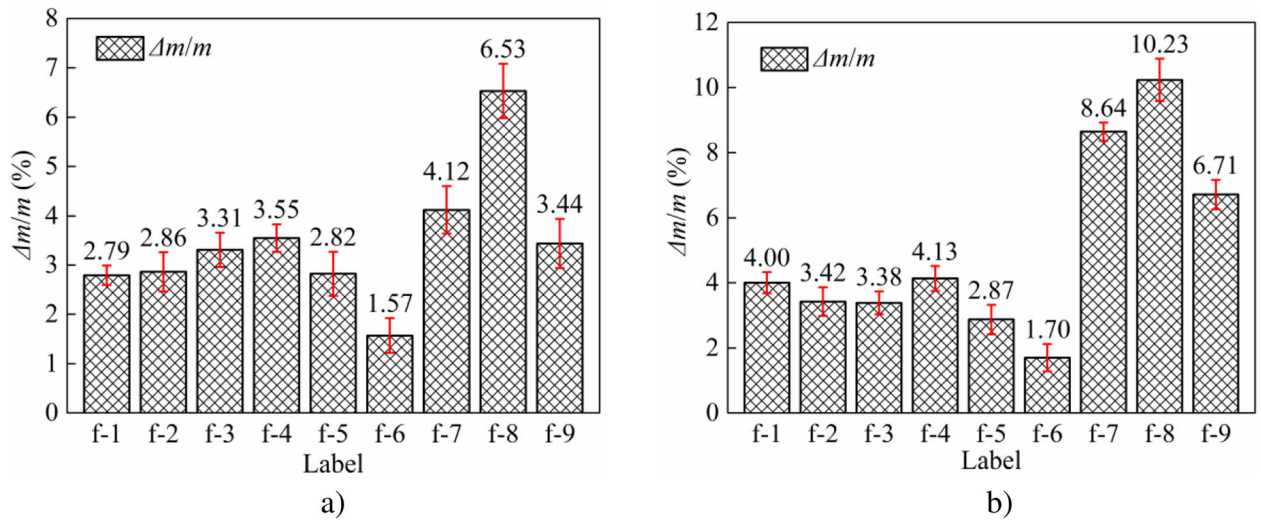

Fig. 5 Mass change of SCGAAC subjected to a different number of freeze-thaw circles: a) after 25 freeze-thaw cycles; and b) after 50 freeze-thaw cycles

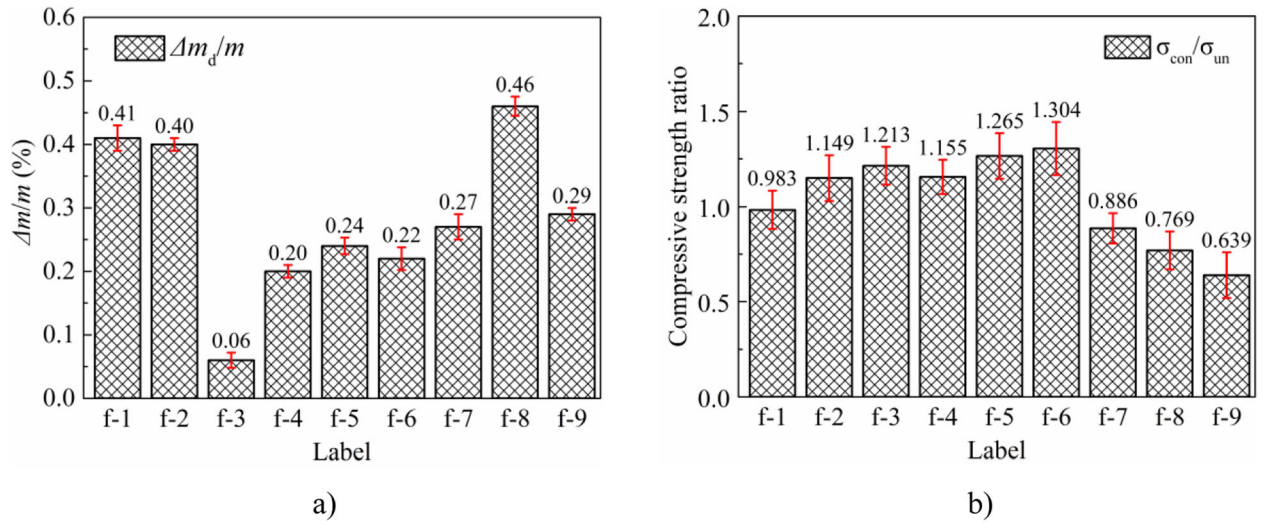

Fig. 6 Difference of SCGAAC subjected to 50 freeze-thaw cycles: a) absolutely dried mass; and b) compressive strength ratio

unsaturated after 72-h water absorption and water kept permeating in the matrix during the following freeze-thaw cycles. That explained the highest mass increment for the samples with calcium stearate. For the other two SCGAAC samples, the mass increment showed a similar level around 3.0%.

Figure 5b) presented the mass change of the SCGAAC after 50 cycles. All of the samples still kept increasing the mass after 50 freeze-thaw cycles, and all of the samples showed intact appearance. The SCGAAC without calcium stearate increased the mass marginally after 50 cycles instead of developing mass loss. The steady mass increase occurred in the SCGAAC comprising calcium stearate, where the highest increment went beyond 10% (f-8). It demonstrated that calcium stearate modified the matrix hydrophobic and controlled the water permeating. CG had strong water absorption ability itself and it was ease for CG to seize surrounding water. Calcium stearate probably changed the surface properties of CG and water infiltrating postponed. Although this blocking effect temporarily slowed water absorption of SCGAAC, the following moisture transport through pore channels was hindered notably.

In order to further examine the difference caused by freeze-thaw cycles, the samples experienced 50 freeze-thaw cycles dried at 105 °C to reach a constant mass. The absolutely dried mass were recorded and the compressive strength were tested, and the corresponding comparisons were shown in Fig. 6. It can be seen, in Fig. 6 (a), the absolutely dried mass change $\Delta m_d/m$ was a positive value for the each sample, which meant growth of the SCGAAC matrix happened. This weight increment likely attributed to cement hydration during the freeze-thaw period. The autoclave curing protocol for the SCGAAC was heating at 196 °C (1.1 MPa) in water vapor for 8 h, during which most precursors would react and generate reaction products. However, CG inclined to hold and consume water as much as possible when the precursors were mixed with water. It took hours for cement particles to hydrate and the free water would be insufficient for complete hydration taking place at that time. The subsequent freeze-thaw tests appropriately supplied water for the unhydrated cement. This was the most likely reason for the absolutely dried weight increment of the SCGAAC.

The compressive strength of the SCGAAC was also different with the counterparts experienced freeze-thaw cycles. The ratios of compressive strength of SCGAAC samples subjected 50 freeze-thaw cycles (σ_{con}) to compressive strength of the original SCGAAC samples (σ_{un}) were presented in Fig. 6 (b). The f-1 to f-6 samples enhanced the compressive strength at different levels while the f-7 to f-9 samples with calcium stearate had a decreased compressive strength. Herein, the freezing processes were performed in air rather than in water, therefore the unsaturated pores supplied sufficient room for releasing frost heaving deformation. Moreover, all of the samples were undamaged visibly and had increased mass. It can be considered that the frost heaving damage of the SCGAAC hardly happened. The decreased compressive strength of the samples possibly resulted from permeation stress as water infiltrated through the waterproof matrix formed by calcium stearate.

Predictive models

On the basis of the test results, the water absorptivity of the SCGAAC could be related to the matrix as well as pore parameters. Herein, the fine pore (<0.5 mm)

fraction and the ALwR were applied to fit a predictive model of water absorptivity of SCGAAC. The proposed model was shown as Eq. (2):

$$W_s = 0.75\ \ln(ALwR) + 0.95P_{0.5} + R_1 \tag{2}$$

where W_s is the 72-h water absorptivity of the SCGAAC; $P_{0.5}$ is the percentage of fine pores (<0.5 mm); and R_1 is a parameter related to effectiveness of chemical agents, equal to 0.1 as no chemical agent being used and equal to 0.15 and 0.12 for foam stabilizer and calcium stearate, respectively. The prediction values from Eq. (2) matched well to the test results. For porous AAC, pore structure strongly influenced water absorptivity. The pores with large diameters hardly contributed to water absorption process, therefor the fraction of those pores with small size were considered to build the proposed model. The isolated pores failed to convey water as an effective driving force during water absorption and the ALwR was used to reflect the effect of pore interconnection on water absorptivity. R_1, a parameter related to material, was applied to show the difference caused by chemical agents.

For the frost resistance performance, compressive strength variation ($\Delta\sigma$) and normalized mass increment ($\Delta m/m$) were chosen as two assessment indexes. Herein, two critical factors, strength-to-density ratio (σ/ρ) and the total porosity (P_t), were used to build the corresponding models. Strength-to-density ratio reflected the effectiveness of matrix as a backbone of porous AAC and pore volume supplied potential room for frost heaving stress transferring. A parameter, R_2, was applied to show the difference caused by chemical agents. R_2 for the SCGAAC without any admixture assigned to a value of 10.8, and R_2 assigned to 10.9 and 10.1 when foam stabilizer and calcium stearate were used respectively. The secondary hydration of cement and influence of chemical agent on mechanical properties were taken into account when assign specific values to the R_2. Accordingly, the compressive strength variation of SCGAAC experiment freeze-thaw cycles can be predicted using Eq. (3):

$$\Delta\sigma = 7.26\ \ln(P_t) - \frac{1}{250 \cdot \sigma/\rho} + R_2 \tag{3}$$

The normalized mass increment of SCGAAC experienced freeze-thaw cycles can be related to the strength-to-density ratio, the fine pore porosity as well as material parameter R_3. These three factors corporately adjusted the normalized mass increment, and assigned the values of 1.10, 1.05 and 0.95 to R_3 for chemical agent free SCGAAC, SCGAAC with foam stabilizer and SCGAAC with calcium stearate, respectively. Eq. (4) was proposed to predict the normalized mass increment of SCGAAC:

$$\frac{\Delta m}{m} = 1.14 \cdot e^{-\frac{\sigma}{\rho}} + \frac{1}{(64 \cdot P_{0.5})^2} - R_3 \tag{4}$$

Figure 7 presented the comparison between the test results and prediction results obtained from Eq. (2) to (4). It can be seen that the proposed models showed similar results to development of the SCGAAC experienced water absorption and freeze-thaw cycles. The model results matched to the test results at a good level. To some extent, the proposed models supplied a guide for SCGAAC design. The water absorption properties and frost resistance performance can be obtained when the basic physic properties of SCGAAC were tested.

Conclusions

Focusing on the water absorptivity and frost resistance performance of SCGAAC, 9 SCGAAC samples with different SF and chemical agents were tested, including porosity, water absorption, and mass change experienced freeze-thaw cycles etc. According to the tests and corresponding analysis, the main conclusions were drawn as follow:

1) Foam stabilizer achieved dense SCGAAC through adjusting surface tension of the slurry to hold more isolated bubbles suspending in the fresh paste. Calcium stearate had an effect on changing hydrophilicity of the matrix material and decreased the density of SCGAAC. Both foam stabilizer and calcium stearate decreased the porosity of SCGAAC effectively.
2) Compressive strength of SCGAAC was influenced by SF and chemical agents. The SCGAAC with SF of 250 mm had high compressive strength. Foam stabilizer almost had no influence on compressive strength while calcium stearate obviously decreased the compressive strength.
3) SCGAAC had high water absorptivity due to the porous matrix and high water uptake capacity of CG. Foam stabilizer slightly increased the water absorption and water absorption rates at any period, while calcium stearate because of the water proof property decreased the water absorption rate.
4) SCGAAC exhibited excellent frost resistance performance. All of the samples kept intact appearance after experiencing 50 freeze-thaw cycles and the absolute dried mass of the samples slightly increased. Most of the SCGAAC developed compressive strength to the higher values and the samples comprising foam stabilizer increased the compressive strength obviously. By contrast, compressive strength of the SCGAAC containing calcium stearate deteriorated.

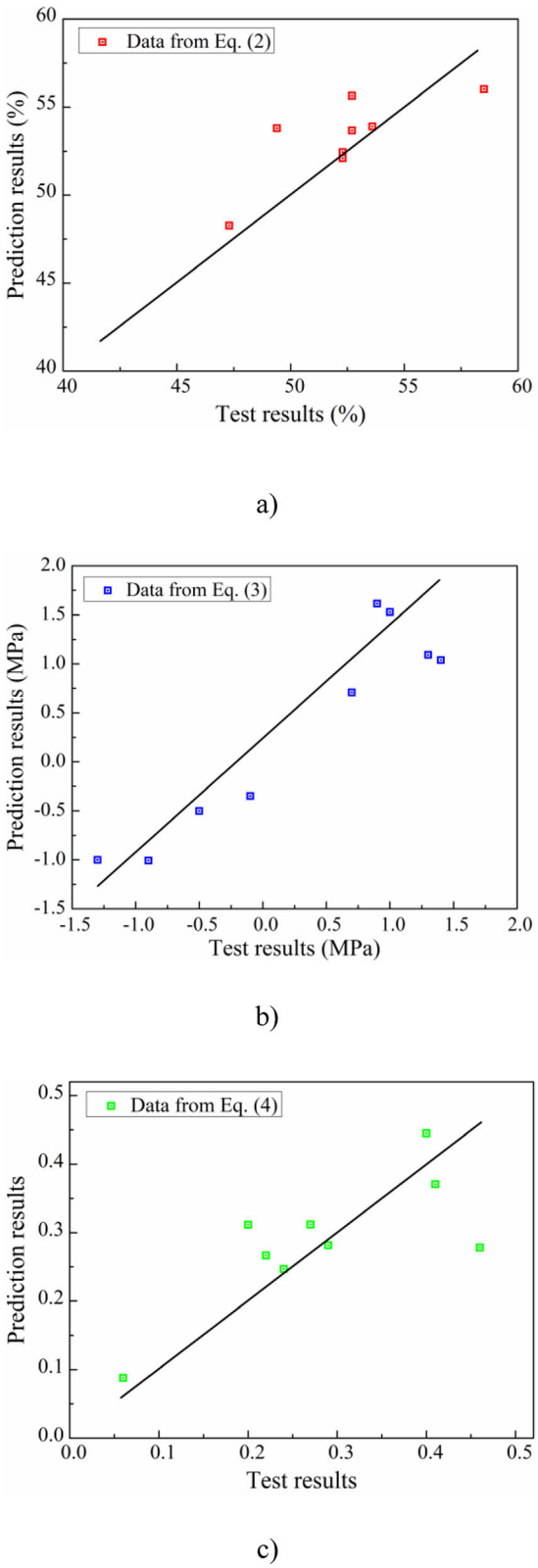

Fig. 7 Comparison between prediction results and test results: a) data from Eq. (2); b) data from Eq. (3); and c) data from Eq. (4)

5) The models proposed for predicting water absorptivity, mass change and strength change matched well to the corresponding test results. These models would reasonably predict water absorption ability and frost resistance performance through some basic physic parameters.

Abbreviations

AAC: Autoclaved aerated concrete; CG: Coal gangue; SCG: Self-ignition coal gangue; SCGAAC: SCG-based AAC; PC: Ordinary Portland cement; L: Lime; G: Gypsum; FDN: Naphthalene-based superplasticizer; SF: Slump flow; AP: Aluminum powder; F: Foam stabilizer; C: Calcium stearate; W/P: Water-to-precursor ratio; ρ: SCGAAC density; SDFM: Super depth of field microscope; ALwR: Average length-width ratio; $\Delta m/m$: Mass change; $\Delta m_d/m$: Absolutely dried mass change; σ_{con}: Compressive strength of SCGAAC samples subjected 50 freeze-thaw cycles; σ_{un}: Compressive strength of original SCGA AC samples; W_s: 72-h water absorptivity; $P_{0.5}$: Percentage of fine pores (<0.5 mm); R_1: Parameter related to effectiveness of chemical agents; σ/ρ: Strength-to-density ratio; P_t: Total porosity; R_2: Parameter relevant to chemical agents; R_3: Material parameter

Acknowledgements

The author acknowledges the editorial assistance and the constructive criticism by the anonymous reviewers.

Authors' contributions

XC performed the design of the study and collection, analysis, and interpretation of data, and was a major contributor in writing the manuscript. YT and SL supervised the entire project. ZW proposed the experimental program. TH helped to conduct laboratory tests and review the manuscript. All authors read and approved the final manuscript.

Funding

The authors would like to acknowledge funding support from Heilongjiang Postdoctoral Fund No. LBH-Z20137 and National Natural Science Foundation of China No. 51872064. The authors also would like to acknowledge the State Key Laboratory of Solid Waste Reuse for Building Materials SWR-2020-005.

Availability of data and materials

Data and materials will be made available upon reasonable request to the corresponding author.

Declarations

Ethics approval and consent to participate

Not applicable.

Consent for publication

Not applicable.

Competing interests

The authors declare that they have no competing interests.

Author details

[1]School of Transportation Science and Engineering, Harbin Institute of Technology, Huanghe Road 73, Harbin 150090, China. [2]School of Civil Engineering, Harbin Institute of technology, Harbin 150090, China. [3]Key Lab of Structures Dynamic Behavior and Control of the Ministry of Education, 9 Harbin Institute of Technology, Harbin 150090, China. [4]State Key Laboratory of Solid Waste Reuse for Building Materials, Beijing Building 11 Materials Academy of Science Research, Beijing 100041, China.

Received: 10 February 2021 Accepted: 28 April 2021
Published online: 11 May 2021

References

1. Wongkeo W, Chaipanich A (2010) Compressive strength, microstructure and thermal analysis of autoclaved and air cured structural lightweight concrete

made with coal bottom ash and silica fume. Mat Sci Eng A struct 527(16-17):3676–3684. https://doi.org/10.1016/j.msea.2010.01.089
2. Yang J, Shi Y, Yang X, Liang M, Li Y, Li Y, Ye N (2013) Durability of autoclaved construction materials of sewage sludge-cement-fly ash-furnace slag. Constr Build Mater 48:398–405. https://doi.org/10.1016/j.conbuildmat.2013.07.018
3. Ungkoon Y, Sittipunt C, Namprakai P, Jetipattaranat W, Kim K, Charinpanitkul T (2007) Analysis of microstructure and properties of autoclaved aerated concrete wall construction materials. J Ind Eng Chem 13:1103–1108
4. Deng M, Zhang W, Yang S (2020) In-plane seismic behavior of autoclaved aerated concrete block masonry walls retrofitted with high ductile fiber-reinforced concrete. Eng Struct 219:110854. https://doi.org/10.1016/j.engstruct.2020.110854
5. Liu R, Huang Y (2018) Heat and moisture transfer characteristics of multilayer walls. Energ Procedia 152:324–329
6. Hussin MW, Muthusamy K, Zakaria F (2010) Effect of mixing constituent toward engineering properties of POFA cement-based aerated concrete. J Mater Civil Eng 22(4):287–295. https://doi.org/10.1061/(ASCE)0899-1561(2010)22:4(287)
7. Drochytka R, Zach J, Korjenic A, Hroudová J (2013) Improving the energy efficiency in buildings while reducing the waste using autoclaved aerated concrete made from power industry waste. Energ Build 58:319–323. https://doi.org/10.1016/j.enbuild.2012.10.029
8. Narayanan N, Ramamurthy K (2000) Structure and properties of aerated concrete: a review. Cement Concrete Comp 22(5):321–329. https://doi.org/10.1016/S0958-9465(00)00016-0
9. Stumm A, Schweike U, Stemmermann P (2018) Nanostructured high insulating autoclaved aerated concrete. MAUERWERK 22(5):329–334. https://doi.org/10.1002/dama.201800024
10. Kalpana M, Mohith S (2020) Study on autoclaved aerated concrete: review. Mater Today Proceed 22:894–896. https://doi.org/10.1016/j.matpr.2019.11.099
11. Jerman M, Keppert M, Výborný J, Černý R (2013) Hygric, thermal and durability properties of autoclaved aerated concrete. Constr Build Mater 41:352–359. https://doi.org/10.1016/j.conbuildmat.2012.12.036
12. Koronthalyova O (2011) Moisture storage capacity and microstructure of ceramic brick and autoclaved aerated concrete. Constr Build Mater 25(2):879–885. https://doi.org/10.1016/j.conbuildmat.2010.06.098
13. Fernández-Jiménez A, Palomo A, Criado M (2005) Microstructure development of alkali-activated fly ash cement: a descriptive model. CEMENT CONCRETE RES 35(6):1204–1209. https://doi.org/10.1016/j.cemconres.2004.08.021
14. Qu X, Zhao X (2017) Previous and present investigations on the components, microstructure and main properties of autoclaved aerated concrete—a review. Constr Build Mater 135:505–516. https://doi.org/10.1016/j.conbuildmat.2016.12.208
15. Ioannou I, Hamilton A, Hall C (2008) Capillary absorption of water and n-decane by autoclaved aerated concrete. Cement Concrete Res 38(6):766–771. https://doi.org/10.1016/j.cemconres.2008.01.013
16. Cong X, Lu S, Yao Y, Wang Z (2016) Fabrication and characterization of self-ignition coal gangue autoclaved aerated concrete. Mater Design 97:155–162. https://doi.org/10.1016/j.matdes.2016.02.068
17. Chinese National Standard (2009) Test methods for performance of autoclaved aerated concrete (GB/T 11969–2008). China building industry press, Beijing

Publisher's Note